Short positron lifetime at vacancies observed in electron-irradiated tungsten: Experiments and first-principles calculations

A. Yabuuchi*, M. Tanaka, A. Kinomura

Institute for Integrated Radiation and Nuclear Science, Kyoto University, Kumatori, Osaka 590–0494, Japan

Abstract

A positron lifetime component of ∼170 ps has been reported for irradiated tungsten (W) in some studies. This value is considerably shorter than that calculated for isolated monovacancies (∼200 ps). In this study, positron annihilation lifetime spectroscopy was used to investigate the recovery behavior of the defects with a short positron lifetime of ∼170 ps in electron-irradiated W. The binding energies and positron lifetimes of vacancy-impurity complexes decorated with impurity atoms were calculated. A positron lifetime of 169 ps, which was similar to the experimentally observed lifetime of 171 ± 1 ps, was calculated for defect complexes comprising a monovacancy decorated with two hydrogen atoms (V-2H complexes). In addition, a value of 1.42 eV was calculated for the dissociation energy of a hydrogen atom from the V-H and V-2H complexes, and the defects with a positron lifetime of ∼170 ps were experimentally observed to migrate at 623 K. These were consistent with previously reported dissociation energy and desorption temperature of deuterium from vacancies in W studied by thermal desorption spectroscopy. These results suggested that the vacancies observed in the electron-irradiated W were hydrogen-decorated V-nH complexes.

Keywords: Tungsten, Electron-irradiation, Vacancy-impurity complex, Dissociation energy, Positron annihilation lifetime spectroscopy, First-principles calculation

1. Introduction

Positron annihilation spectroscopy is a useful technique for investigating vacancy-type defects in crystalline materials [1, 2, 3] and has also been widely used to study irradiation-induced vacancies formed in tungsten (W). Several experimental studies have reported a positron lifetime component of 189–200 ps for irradiated W [4, 5, 6]. This value is comparable to that (193–200 ps) calculated for isolated monovacancies in W [7, 8, 9]. However, some experimental studies on irradiated W have reported a positron lifetime component of 169–175 ps [9, 10, 11], which is significantly shorter than that calculated for isolated monovacancies.

In this study, we focused on the short positron lifetime observed for irradiated W. Well-annealed W samples were prepared for positron annihilation lifetime (PAL) measurements, and a portion of the samples was irradiated with electrons to introduce vacancy-type defects. With respect to several possible impurity elements in W, positron lifetimes for defect complexes, which comprise a monovacancy decorated with an impurity atom, were calculated and compared with the experimentally obtained values. The binding and dissociation energies of such vacancy-impurity complexes were also evaluated. The electron-irradiated W was isochronally annealed to investigate the recovery temperature of defects with a short positron lifetime. Furthermore, the recovery temperature was compared with that of isolated monovacancies reported in other positron annihilation studies [12, 13] and with previously reported thermal desorption spectroscopy (TDS) data obtained for W [14, 15]. Eventually, the species of defects having the short positron lifetime observed in the electron-irradiated W was deduced.

2. Experimental method

Four pieces of 5 × 10 mm^2 samples were cut from a 0.8-mm-thick sintered W plate (nominal purity: 99.999%; Metal Technology Co. Ltd.). After mechanical polishing, samples were annealed under vacuum (10^{-4} Pa) for 15 min at a temperature of ∼2473 K using an electron-bombardment heating technique [16]. Two pieces of the annealed samples were then irradiated with 8-MeV electrons using an electron linear accelerator at the Institute for Integrated Radiation and Nuclear Science, Kyoto University (KURNS-LINAC). Figure 1 shows a schematic of the electron irradiation performed on the samples. The two pieces of samples were placed side-by-side (without overlapping) and vacuum-encapsulated in a 0.5-mm-thick aluminum (Al) capsule. The vacuum-encapsulation of the samples was performed by pressure-bonding and cutting the capsule that was being evacuated by an oil-

*Corresponding author
Email address: yabuuchi@rri.kyoto-u.ac.jp (A. Yabuuchi)

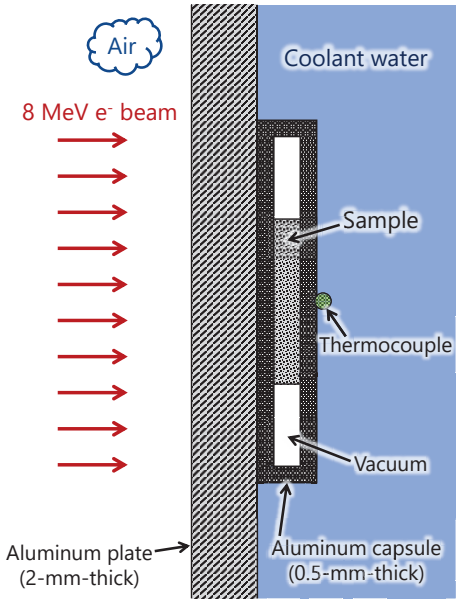

Figure 1: Schematic showing electron irradiation. Two pieces of samples were placed side-by-side (without overlapping) and simultaneously irradiated.

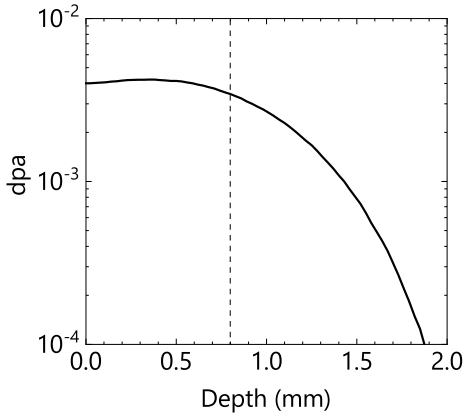

Figure 2: Depth distribution of displacement per atom (dpa) in W irradiated with 8-MeV electrons through a 2.5-mm-thick Al. The vertical dashed line indicates the actual thickness of the W sample used in this study. The dpa profile was calculated using the PHITS code.

sealed rotary vacuum pump. The capsule was mounted on an Al water-cooled sample holder and irradiated with 8-MeV electrons through a 2-mm-thick Al plate (dose rate: 2.5×10^{14} e^-/cm^2s, total dose: 5×10^{19} e^-/cm^2; Fig. 1). Figure 2 shows the depth distribution of displacement per atom (dpa) in the W sample irradiated with 8-MeV electrons through the 2.5-mm-thick Al (*i.e.*, the 2-mm-thick plate and the 0.5-mm-thick capsule). The distribution was calculated using the PHITS 3.20 code [17, 18, 19]. The irradiation damage was estimated to be formed almost uniformly throughout the 0.8-mm-thick W sample. Moreover, the sample's temperature was measured by a thermocouple installed on the back surface of the capsule, as shown in Fig. 1, and a temperature of ∼373 K was measured during the electron irradiation. After the irradiation, samples were carefully picked up from the capsule without deforming them. No liquid water intrusion was visible in the capsule that opened after the irradiation.

The irradiated samples were then placed on a quartz boat and isochronally annealed under vacuum (10^{-4} Pa) using an electric furnace. Each annealing was performed for 15 min at temperatures ranging from 323 K to 1423 K (temperature step: 50 K). After each annealing step, PAL measurements were performed at room temperature. PAL spectra were acquired through a conventional γ-γ coincidence PAL measurement technique [1] using a digital oscilloscope (Teledyne LeCroy WaveSurfer 510) and two photomultiplier tubes (Hamamatsu H3378-51) with a BaF_2 scintillator. The positron source was a 7.5-μm-thick Kapton-foil-sealed ^{22}NaCl with an intensity of ∼1 MBq. The sealed positron source was sandwiched between two pieces of samples to ensure that all positrons emitted from the source in any direction are incident on the samples. In each measurement, the incident face of the positrons was always the same as that of the 8-MeV electrons. More than 1×10^6 annihilation events were accumulated for each PAL spectrum with a time resolution of 200 ps (full width at half maximum).

The acquired PAL spectra $T(t)$ were analyzed using the PALSfit3 program [20, 21]. The source-contributed components were 386 ps and 2 ns with corresponding intensities of ∼22% and ∼1%, respectively. After correcting for the source components and background, $T(t)$ was decomposed into two exponential terms:

$$T(t) = \frac{I_1}{\tau_1} \exp\left(-\frac{t}{\tau_1}\right) + \frac{I_2}{\tau_2} \exp\left(-\frac{t}{\tau_2}\right), \qquad (1)$$

where τ_1 and τ_2 represent shorter and longer positron lifetime components, and I_1 and I_2 are the corresponding relative intensities. The total intensity of the two components is unity ($I_1 + I_2 = 100\%$). A mean positron lifetime τ_M was also derived by analyzing the PAL spectrum $T(t)$ as a single exponential term:

$$T(t) = \frac{1}{\tau_M} \exp\left(-\frac{t}{\tau_M}\right). \qquad (2)$$

Let us consider the PAL spectrum analysis with fitting to one or two exponential components. The variance of fit was evaluated using the χ^2/ndf value obtained by dividing the square sum of fitting differences χ^2 by the number of degrees of freedom (ndf). In the PAL spectra analysis, the χ^2/ndf value close to unity shows good fitting. The value greater than unity shows poor fitting, in other words, it suggests the presence of additional lifetime components in the spectrum. The value considerably less than unity shows that the analysis is overfitting.

Based on the two-state trapping model [22, 23, 24], which assumes that only one defect species is present in the sample, τ_2 is related to the positron lifetime at defects

($\tau_2 = \tau_{\rm D}$). The positron trapping rate of defects κ is given as follows:

$$\kappa = \left(\frac{I_2}{I_1}\right)\left(\frac{1}{\tau_{\rm B}} - \frac{1}{\tau_2}\right), \tag{3}$$

where $\tau_{\rm B}$ and τ_2 are the positron lifetimes of a defect-free lattice (bulk) and defects, respectively. According to the two-state trapping model, the shorter positron lifetime τ_1 is represented as

$$\tau_1 = \frac{1}{\lambda_{\rm B} + \kappa}, \tag{4}$$

where $\lambda_{\rm B}$ is the annihilation rate of delocalized positrons, which is given by the reciprocal of $\tau_{\rm B}$ ($\lambda_{\rm B} = \tau_{\rm B}^{-1}$). When defects are present, the observed τ_1 becomes shorter than $\tau_{\rm B}$ due to positron trapping of the defects, as seen from Eq. (4). From Eqs. (3) and (4), the shorter positron lifetime component τ_1, which satisfies the two-state trapping model, can be derived from the observed values of I_1 ($= 1 - I_2$), I_2, and τ_2. In this paper, τ_1 derived from the two-state trapping model is denoted as $\tau_1^{\rm TM}$. If the experimentally observed τ_1 is longer than the calculated $\tau_1^{\rm TM}$, this indicates that other defect species with a positron lifetime shorter than τ_2 are present in the sample. In this case, the reason why τ_1 becomes longer than $\tau_1^{\rm TM}$ is that the lifetime component of positrons annihilated at defects, which have a shorter positron lifetime than τ_2, cannot be separated from that of delocalized positrons.

3. Computational method

Binding energies between a monovacancy and an impurity atom, as well as positron lifetimes for the vacancy-impurity complexes, were calculated using the first-principles calculation code ABINIT 8.10.1 [25, 26, 27, 28, 29], which is based on the density functional theory (DFT). The electron-ion interaction was described using a projector-augmented wave potential [30], and the exchange-correlation functional between electrons was based on the generalized gradient approximation of Perdew, Burke, and Ernzerhoff [31]. Positron lifetimes were calculated using a two-component DFT calculation scheme [32, 33] with the local density approximation of Puska, Seitsonen, and Nieminen [34] as the electron-positron exchange-correlation functional. Body centered cubic supercells with a size of $3 \times 3 \times 3$ (54 atoms in perfect lattice) were used in the calculations. The cutoff energy of the plane-wave and k-point sampling mesh were 218 eV and a $6 \times 6 \times 6$ mesh, respectively. The total energies of the supercells characterizing each defect structure were obtained by iterating lattice-relaxation calculations until the force acting on each atom became less than 2.6×10^{-3} eV/Å. In the positron lifetime calculations, the above-mentioned relaxed structures were used as the initial structures. The lattice-relaxation calculations were then iterated again until the force acting on each atom became less than 2.6×10^{-3} eV/Å when a positron was localized to the vacancy-type defects. The VESTA 3.4.6 code [35] was used to plot the atomic configurations and positron density distributions.

In this paper, the following elements are listed as examples of possible impurities in W [36]: hydrogen (H), carbon (C), nitrogen (N), oxygen (O), tantalum (Ta), molybdenum (Mo), iron (Fe), and phosphorus (P). The former four and latter four elements are interstitial and substitutional impurities, respectively. Binding energies and positron lifetimes were calculated for the vacancy-impurity complexes associated with these impurity elements. Figure 3 shows representative examples of the calculated defect structures. Stable positions for each isolated interstitial impurity atom were confirmed through the calculations of the cases corresponding to the location of the impurity atom at the tetrahedral center (T-site) and the octahedral center (O-site) (Figs. 3(a) and (b)). In the calculations of the vacancy-impurity complexes associated with interstitial impurities, the impurity atom was initially placed at the O-site (Fig. 3(c)), which would be near the most stable position [37]. The atomic configurations with two (or three) H atoms at two (or three) O-sites near a vacancy were also calculated but only in the case of hydrogen (Fig. 3(d–e)). For the vacancy-impurity complexes associated with substitutional impurities, the impurity atom substituted the W atom in the first nearest neighbor of a vacancy, as shown in Fig. 3(f).

The binding energies $E^{\rm B}_{V\text{-}{\rm X_I}}$ between the monovacancy (V) and the interstitial impurity atom ($\rm X_I$) and $E^{\rm B}_{V\text{-}{\rm X_S}}$ between V and the substitutional impurity atom ($\rm X_S$) were determined from:

$$E^{\rm B}_{V\text{-}{\rm X_I}} = -\Big[\big\{E({\rm W_{54}}) + E({\rm W_{53}X_I})\big\} - \big\{E({\rm W_{53}}) + E({\rm W_{54}X_I})\big\}\Big], \tag{5}$$

$$E^{\rm B}_{V\text{-}{\rm X_S}} = -\Big[\big\{E({\rm W_{54}}) + E({\rm W_{52}X_S})\big\} - \big\{E({\rm W_{53}}) + E({\rm W_{53}X_S})\big\}\Big], \tag{6}$$

where $E({\rm W_{54}})$, $E({\rm W_{53}X_I})$, $E({\rm W_{53}})$, $E({\rm W_{54}X_I})$, $E({\rm W_{52}X_S})$, and $E({\rm W_{53}X_S})$ are the total energies of the supercells associated with the perfect lattice, V-$\rm X_I$ complex, isolated V, isolated $\rm X_I$, V-$\rm X_S$ complex, and isolated $\rm X_S$, respectively. For the isolated interstitial impurity atom, the total energies of both supercells with arranging the impurity atom at the T- or O-sites were calculated, and the smaller one was adopted as $E({\rm W_{54}X_I})$. The binding energy $E^{\rm B}_{V{\rm H\text{-}H}}$ between the V-H complex and the H atom, *i.e.*, the binding energy of the second H atom at a vacancy, was calculated as follows:

$$E^{\rm B}_{V{\rm H\text{-}H}} = -\Big[\big\{E({\rm W_{54}}) + E({\rm W_{53}H_2})\big\} - \big\{E({\rm W_{53}H}) + E({\rm W_{54}H})\big\}\Big], \tag{7}$$

where $E({\rm W_{53}H_2})$, $E({\rm W_{53}H})$, and $E({\rm W_{54}H})$ are the total

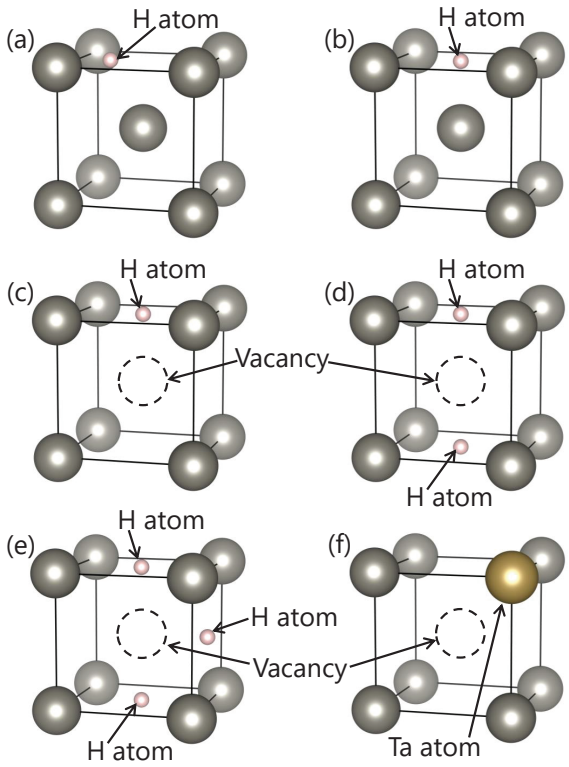

Figure 3: Representative examples of the defect structures calculated in this study. H and Ta atoms are depicted as representatives of interstitial and substitutional impurity atoms, respectively. All atomic configurations shown here are depicted in an unrelaxed state. (a) Isolated interstitial impurity atom at T-site. (b) Isolated interstitial impurity atom at O-site. (c) Interstitial-impurity-related vacancy-impurity complex. (d) Vacancy-hydrogen complex with two H atoms. (e) Vacancy-hydrogen complex with three H atoms. (f) Substitutional-impurity-related vacancy-impurity complex.

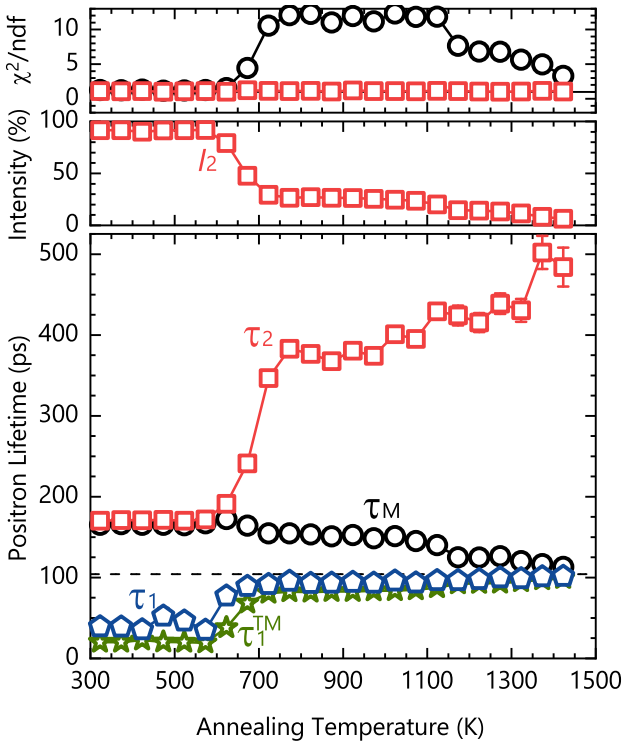

Figure 4: Positron lifetimes ($\tau_{\rm M}$, τ_1, and τ_2), intensity (I_2), and χ^2/ndf values obtained for the electron-irradiated sample as a function of annealing temperature. The χ^2/ndf values represented by open circles and open squares are values obtained from analysis of the PAL spectra as one- and two-exponential components, respectively. The calculated shorter positron lifetime components ($\tau_1^{\rm TM}$) based on the two-state trapping model are indicated as open stars. The positron lifetime of 104 ps obtained for the unirradiated sample annealed at 2473 K is denoted by the horizontal dashed line.

energies of the supercells associated with the V-2H complex, V-H complex, and isolated H atom, respectively. In a similar way, the $E^{\rm B}_{V{\rm H}_2\text{-H}}$ between the V-2H complex and the third H atom was calculated as follows:

$$E^{\rm B}_{V{\rm H}_2\text{-H}} = -\Big[\big\{E({\rm W}_{54}) + E({\rm W}_{53}{\rm H}_3)\big\} - \big\{E({\rm W}_{53}{\rm H}_2) + E({\rm W}_{54}{\rm H})\big\}\Big], \quad (8)$$

where $E({\rm W}_{53}{\rm H}_3)$ is the total energy of the supercell associated with the V-3H complex.

4. Results

4.1. Experimental results

Only a single positron lifetime component of 104 ps is obtained for the unirradiated sample after annealing at 2473 K. Figure 4 shows the isochronal annealing behavior of positron lifetimes ($\tau_{\rm M}$, τ_1, τ_2, and $\tau_1^{\rm TM}$), intensity (I_2), and χ^2/ndf (corresponding to one- and two-component analysis) obtained for the irradiated sample. The χ^2/ndf values in the one-component analysis are larger than unity over the entire temperature range, and the PAL spectra can be decomposed into two components. The longer positron lifetime component τ_2 is 170 ps (intensity I_2: 91%) at 323 K and remains at 171 ± 1 ps (I_2: 91 ± 1%) up to 573 K. At 623–773 K, the χ^2/ndf value in the one-component analysis and τ_2 increase significantly, whereas I_2 decreases considerably. The τ_2 value increases gradually to ∼450–500 ps at temperatures above 773 K and the corresponding intensity I_2 decreases.

However, the shorter positron lifetime component at 323 K (*i.e.*, $\tau_1 = 39$ ps) is significantly longer than the $\tau_1^{\rm TM}$ (20 ps) derived from the two-state trapping model. The difference between τ_1 and $\tau_1^{\rm TM}$ persists to a temperature of at least 673 K. In the high-temperature range (above 1173 K), τ_1 and $\tau_1^{\rm TM}$ are nearly identical.

4.2. Computational results

The calculated binding energies $E^{\rm B}_{V\text{-X}}$ and positron lifetimes τ of the vacancy-impurity complexes are summarized in Table 1. The calculation results indicate that the binding energies between a monovacancy and an interstitial impurity atom (H, C, N, and O) are substantially larger than those of substitutional impurity atoms (Ta, Mo, Fe, and P). In addition, the value of the binding energy between

Table 1: Calculated binding energies $E^{\mathrm{B}}_{V\text{-X}}$ and positron lifetimes τ of vacancy-impurity complexes. Positron lifetimes calculated for a perfect lattice and isolated monovacancies are also indicated.

Defect Species	$E^{\mathrm{B}}_{V\text{-X}}$ (eV)	τ (ps)
Perfect Lattice	—	101
Isolated V	—	195
V-H	1.21	184
VH-H (V-2H)	1.21	169
VH$_2$-H (V-3H)	1.04	164
V-C	2.19	171
V-N	2.89	170
V-O	3.92	168
V-Ta	0.06	195
V-Mo	0.04	196
V-Fe	0.19	199
V-P	0.69	200

the V-H complex and the second H atom is indicated to be comparable to that between the isolated V and H atom. The binding energy $E^{\mathrm{B}}_{V\mathrm{H_2}\text{-H}}$ between the V-2H complex and the third H atom is derived to be 1.04 eV, which is slightly less than the 1.21 eV for $E^{\mathrm{B}}_{V\text{-H}}$ and $E^{\mathrm{B}}_{V\text{H-H}}$.

Positron lifetimes of 101 and 195 ps are calculated for a defect-free perfect lattice and isolated monovacancies, respectively. Figure 5 shows the calculated positron density distributions of an isolated monovacancy and various vacancy-impurity complexes. For vacancy-impurity complexes comprising a substitutional impurity atom, such as Ta, the localized state of the positron is barely affected, as shown in Fig. 5(e). The calculated positron lifetimes of the substitutional-impurity-related vacancy-impurity complexes are similar to, or only slightly longer than, that of isolated monovacancies, as shown in Table 1. In contrast, the density distributions of the localized positron at a vacancy are distorted, owing to the presence of the interstitial impurity atom (Fig. 5(b–d)). A positron lifetime of ∼170 ps is calculated for the V-C, V-N, and V-O complexes. The corresponding lifetime calculated for the V-H complex (184 ps) is shortened to 169 ps (V-2H) and 164 ps (V-3H) by decorating a vacancy with two or three H atoms.

5. Discussion

The experimental and calculated values of 103–105 ps [38, 39, 40, 41] and 101–108 ps [7, 8], respectively, have been reported for the positron lifetime of a defect-free W lattice. The positron lifetime of 104 ps, detected as a single component from the unirradiated sample, is comparable to the previously reported values for a defect-free W lattice, and hence, the initial defects are considered sufficiently eliminated via annealing. Furthermore, the positron lifetime for isolated monovacancies calculated in this study (195 ps) is comparable to the values reported in previous computational studies (193–200 ps) [7, 8, 9].

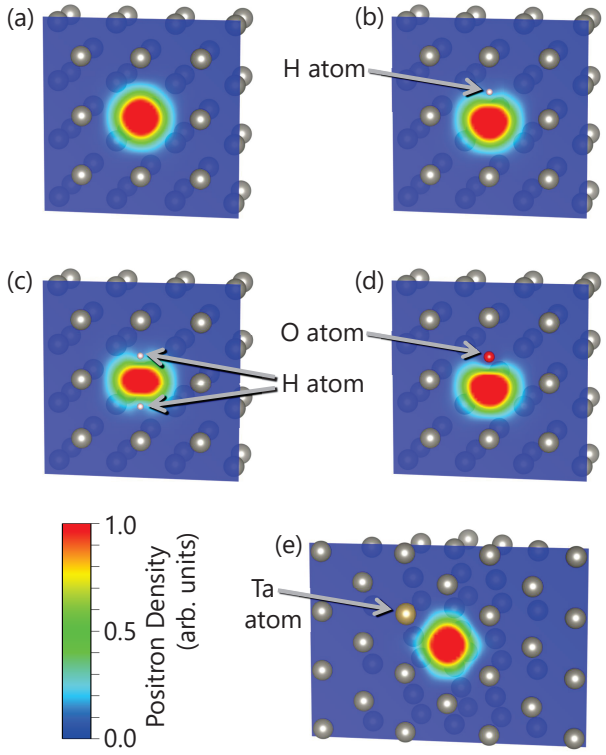

Figure 5: Calculated positron density distributions in (a) isolated V, and in (b) V-H, (c) V-2H, (d) V-O, and (e) V-Ta complexes. The lattices in (a–d) and (e) are cut off on the (001) and (011) planes, respectively. The atomic positions are depicted as spheres.

However, the vacancy-related positron lifetime of $\tau_2 = 171 \pm 1$ ps observed for the electron-irradiated sample at temperatures below 573 K is considerably shorter than the calculated values for isolated monovacancies. Table 2 shows the vacancy-related positron lifetimes reported in previous irradiation studies on W [4, 5, 6, 9, 10, 11, 13]. Some studies [9, 10, 11], including the present one, have reported vacancy-related positron lifetimes, which are significantly shorter than the value calculated for isolated monovacancies. Positron lifetime calculations for the V-X complexes summarized in Table 1 show that the decoration of a monovacancy with C, N, or O atom shortens the respective positron lifetimes to ∼170 ps. In addition, the calculated positron lifetime of the V-2H complexes becomes ∼170 ps.

As vacancies in W undergo almost no migration at the present irradiation temperature (∼373 K) [12, 13], impurity atom diffusion into the vacancies is required for the formation of V-X complexes during irradiation. Previous studies based on first-principles calculations have reported migration energies (diffusion barriers) $E^{\mathrm{M}}_{\mathrm{X}}$ of 0.21, 1.46, 0.72, and 0.17 eV for H, C, N, and O atoms, respectively, in the W lattice [43, 44, 45, 46, 47]. According to these studies, the diffusion coefficients D_{X} of H, C, N, and O atoms in the W lattice are given as follows:

$$D_{\mathrm{H}} = 5.2 \times 10^{-8} \exp\left(-E^{\mathrm{M}}_{\mathrm{H}}/kT\right) \quad \mathrm{m}^2/\mathrm{s}, \qquad (9)$$

Table 2: Vacancy-related positron lifetimes reported in previous irradiation studies on W. Irradiated particles and the corresponding energy, sample purity, total dose, dpa, irradiation temperature, irradiation atmosphere, and measurement technique in each experiment are also summarized.

Particles & Energy	Sample Purity (wt%)	Total Dose (cm^{-2})	dpa	Irrad. Temp. (K)	Irrad. Atmos.	Meas. Technique	V-Related Lifetime (ps)	Ref.
8 MeV e^-	99.999	5×10^{19}	4×10^{-3}	∼373	water[a]	conv.	171 ± 1	this work
8.5 MeV e^-	99.99	—	1×10^{-3}	∼373	—	conv.	169	[10]
8 MeV e^-	99.95	9.4×10^{17}	3.2×10^{-5}	333	water	conv.	173 ± 4	[11]
8 MeV e^-	99.95	6.6×10^{18}	6.4×10^{-4}	363 ± 10	water	conv.	∼175[b]	[9]
e^-	—	—	—	300	—	—	180	[42]
10 MeV p^+	99.95	1×10^{16}	—	35	—	conv.	180 ± 15	[13]
21.6 MeV p^+	99.97	5×10^{15}	(1–2)$\times 10^{-5}$	∼373	air	conv.	189 ± 3	[5]
22.5 MeV p^+	99.97	2×10^{16}	6.4×10^{-5}	RT	vacuum	conv.	192 ± 2	[6]
800 keV $^3He^+$	99.95	5×10^{16}	1×10^{-1}	< 333	—	slow e^+	200 ± 0.4	[4]

conv.—conventional positron annihilation lifetime spectroscopy (PALS) using a ^{22}Na positron source.
slow e^+—PALS using a pulsed slow positron beam.
[a] The sample was vacuum-sealed in an Al capsule.
[b] Prior to the measurement, annealing at 573 K was performed for 240 h.

$$D_C = 2.56 \times 10^{-7} \exp\left(-E_C^M/kT\right) \text{ m}^2/\text{s}, \quad (10)$$

$$D_N = 1.66 \times 10^{-7} \exp\left(-E_N^M/kT\right) \text{ m}^2/\text{s}, \quad (11)$$

$$D_O = 7.57 \times 10^{-8} \exp\left(-E_O^M/kT\right) \text{ m}^2/\text{s}, \quad (12)$$

where k and T are the Boltzmann constant and absolute temperature, respectively. Taking the diffusion length as $\sqrt{2D_X t}$ (where t is time), the diffusion lengths of H, C, N, and O atoms in a second at 373 K are 12 μm, 1×10^{-4} nm, 8 nm, and 28 μm, respectively. The estimated diffusion lengths show that the H and O atoms can easily reach vacancies during the irradiation process, whereas the C atoms undergo almost no migration. The N atoms may also reach vacancies because the irradiation process in this study lasted for ∼50 h. When these interstitial impurity atoms encounter vacancies during irradiation, they remain trapped in the vacancies due to the large atom/vacancy binding energy, as summarized in Table 1. From the above, the formation of (for example) V-nH and/or V-O complexes during irradiation is quite possible, implying that these complexes comprise the observed defects with a positron lifetime of ∼170 ps. However, since the difference in the calculated positron lifetimes for V-H, V-2H, and V-3H complexes (in particular the difference between the V-2H and V-3H) is not large, these lifetime components may be observed as τ_2 without being separated.

At temperatures below 573 K, where τ_2 remains at 171 ± 1 ps, the observed τ_1 is clearly longer than the τ_1^{TM} derived from the two-state trapping model. This indicates that, besides the defects associated with τ_2 (∼170 ps), the sample contains other defect species with a positron lifetime shorter than τ_2. Dislocations (in general) induce an intermediate positron lifetime that lies between the respective values obtained for isolated monovacancies and a perfect lattice. Previous experimental studies have reported positron lifetimes of 149 ± 1 ps [11], 153 ± 2 ps [40], and 163 ± 7 ps [6] for dislocations in W. Although no dislocation-induced positron lifetime component was detected in the unirradiated sample, electron irradiation can lead to the formation of interstitial dislocation loops besides vacancies [48]. Besides, more than six H atoms can be trapped in a monovacancy in W [49]. A previous study has reported that the calculated positron lifetimes for V-4H, V-5H, and V-6H complexes as 153, 145, and 142 ps, respectively [9]. As well as dislocations, these defect complexes bring positron lifetimes that are shorter than τ_2. Thus, the observed longer τ_1 might be caused by the mixture of the previously described positron lifetime component, which is shorter than ∼170 ps with the lifetime component of positrons that annihilate in the delocalized state.

In this study, τ_2 begins to increase at 623 K (Fig. 4), which is slightly higher than the migration temperature of isolated monovacancies in W (∼550 K) reported in previous studies using positron annihilation spectroscopy [12, 13]. This suggests that the V-X_I complexes formed during the irradiation begin to dissociate at this temperature. Previous studies based on TDS have shown that the deuterium atoms trapped in vacancies are desorbed at ∼600 K [14, 15]. The calculated binding energies $E^B_{V\text{-H}}$ and $E^B_{V\text{H-H}}$ of the V-H and VH-H complexes obtained in the present study are both 1.21 eV, and the calculated migration energy E^M_H of H is 0.21 eV as reported in reference [43]. From these values, a value of 1.42 eV is estimated for the dissociation energies ($E^B + E^M$) of the H atom from V-H and V-2H complexes. This value is somewhat smaller than the deuterium-vacancy dissociation energy (1.56±0.06 eV) reported in a recent TDS study [15], but is quite close to the value (1.45 eV) reported in another TDS study [14]. Therefore, vacancies decorated with one or more H atoms, *i.e.*, V-nH complexes, are expected to be present in the irradiated sample prepared in this study, and the increase

in τ_2 at 623 K may reflect the dissociation of the V-H and V-2H complexes.

The dissociation energy ($E^{\mathrm{B}} + E^{\mathrm{M}}$) of the H atom from the V-3H complex is estimated to be 1.25 eV, which is slightly less than those of V-H and V-2H complexes (1.42 eV). The binding energies of an H atom to the V-3H, V-4H, and V-5H complexes have been reported in previous computational studies to be smaller than those in the cases of V-H and V-2H complexes [49, 50, 51]. Thus the dissociation energies of the H atom from the V-4H, V-5H, and V-6H complexes are also expected to be even smaller compared with the cases of the V-H, V-2H, and V-3H complexes. The H atoms are expected to be desorbed from the V-nH ($n \geq 3$) complexes at temperatures lower than the dissociation temperature of the V-H and V-2H complexes. However, these V-nH ($n \geq 3$) complexes would eventually become V-2H complexes by releasing H atoms and would be stable up to 623 K, where τ_2 begins to increase. On the other hand, dissociation of the other interstitial impurity elements from vacancies is unfavorable at 623 K because the dissociation energies ($E^{\mathrm{B}} + E^{\mathrm{M}}$) of these elements are considerably larger than that of the H atom.

These H atoms may have originated from not only those that were initially present but also may have been introduced during irradiation. No liquid water intrusion was visible in the Al capsule that opened after irradiation. However, the capsule was vacuum-sealed by pressure-bonding and cannot be said to have been completely free of water contamination. Since the capsule has an exceedingly small internal volume, a small amount of water contamination would greatly degrade the vacuum inside the capsule. To clarify the effect of the contamination during irradiation, the sample might be necessary to be placed in a large vacuum chamber rather than the small capsule and irradiated with evacuating by a vacuum pump.

Figure 4 also shows that τ_2, which is 172 ps at 573 K, increases sharply to 383 ps at 773 K. This is reflective of vacancy aggregation (the vacancies can migrate freely above 623 K), which leads to vacancy-cluster formation. According to a previous study [7], vacancy clusters comprising 9–13 monovacancies are characterized by a positron lifetime of 383 ps. Furthermore, the τ_2 value increases to nearly 500 ps at 1423 K (intensity I_2: ∼6%), but some of the defects induced by the electron irradiation remain.

6. Conclusion

In this study, we focused on defects observed in electron-irradiated W that have a shorter positron lifetime than monovacancies. The experimental and calculated positron lifetimes were compared, and subsequently, the formation of vacancy-impurity complexes decorated with interstitial impurity atoms was predicted. The isochronal annealing behavior of the longer positron lifetime component τ_2 and calculation results of dissociation energies of vacancy-impurity complexes were then compared with previously reported TDS experimental data. The comparison suggested the observed short positron lifetime of ∼170 ps was attributed to hydrogen-related V-nH complexes. The observed value of ∼170 ps corresponds to the calculated positron lifetime of V-2H (169 ps). Estimating the dissociation energies of each impurity element from a vacancy implied that the complexes of the vacancy decorated with other interstitial impurities (*e.g.*, C, N, and O atoms) are not the dominant defects. In the future, experiments and calculations of the Doppler broadening of the annihilation radiation may help to directly identify the elements that decorate the vacancies.

Data availability

The raw/processed data required to reproduce these findings cannot be shared at this time due to technical or time limitations.

Acknowledgments

The authors thank K. Ohsawa (Kyushu Univ.) and T. Yoshiie (Kyoto Univ.) for their useful discussions. We also thank N. Abe (Kyoto Univ.) for technical assistance with the electron-irradiation experiments. We are grateful to S. Makimura (KEK) for providing the high-purity tungsten used in this study. We would like to thank H. Araki, M. Mizuno, and K. Sugita (Osaka Univ.) for their assistance in the sample cutting and for their practical advice on setting up the positron annihilation lifetime spectrometer using a digital oscilloscope. This work was financially supported by Japan Society for the Promotion of Science (JSPS) KAKENHI Grant Number JP17K14896.

References

[1] P. Hautojärvi (Ed.), Springer, Berlin, 1979.
[2] F. Tuomisto, I. Makkonen, Rev. Mod. Phys. 85 (2013) 1583.
[3] J. Čížek, J. Mater. Sci. Technol. 34 (2018) 577.
[4] P. E. Lhuillier, M. F. Barthe, P. Desgardin, W. Egger, P. Sperr, Phys. Status Solidi C 6 (2009) 2329.
[5] O. V. Ogorodnikova, L. Y. Dubov, S. V. Stepanov, D. Terentyev, Y. V. Funtikov, Y. V. Shtotsky, V. S. Stolbunov, V. Efimov, K. Gutorov, J. Nucl. Mater. 517 (2019) 148.
[6] O. V. Ogorodnikova, M. Majerle, V. V. Gann, J. Čížek, P. Hruška, S. Simakov, J. Nucl. Mater. 525 (2019) 22.
[7] T. Troev, E. Popov, P. Staikov, N. Nankov, T. Yoshiie, Nucl. Instrum. Methods Phys. Res. Sect. B 267 (2009) 535.
[8] P. Staikov, N. Djourelov, Physica B 413 (2013) 59.
[9] K. Sato, A. Hirosako, K. Ishibashi, Y. Miura, Q. Xu, M. Onoue, Y. Fukutoku, T. Onitsuka, M. Hatakeyama, S. Sunada, T. Yoshiie, J. Nucl. Mater. 496 (2017) 9.
[10] T. Toyama, K. Ami, K. Inoue, Y. Nagai, K. Sato, Q. Xu, Y. Hatano, J. Nucl. Mater. 499 (2018) 464.
[11] K. Sato, R. Tamiya, Q. Xu, H. Tsuchida, T. Yoshiie, Nucl. Mater. Energy 9 (2016) 554.
[12] A. Debelle, M. F. Barthe, T. Sauvage, J. Nucl. Mater. 376 (2008) 216.
[13] J. Heikinheimo, K. Mizohata, J. Räisänen, T. Ahlgren, P. Jalkanen, A. Lahtinen, N. Catarino, E. Alves, F. Tuomisto, APL Mater. 7 (2019) 021103.

[14] O. V. Ogorodnikova, B. Tyburska, V. K. Alimov, K. Ertl, J. Nucl. Mater. 415 (2011) S661.
[15] M. Zibrov, S. Ryabtsev, Y. Gasparyan, A. Pisarev, J. Nucl. Mater. 477 (2016) 292.
[16] A. Yabuuchi, N. Oshima, H. Kato, B. E. O'Rourke, A. Kinomura, T. Ohdaira, Y. Kobayashi, R. Suzuki, JJAP Conf. Proc. 2 (2014) 011102.
[17] H. Iwase, K. Niita, T. Nakamura, J. Nucl. Sci. Technol. 39 (2002) 1142.
[18] T. Sato, K. Niita, N. Matsuda, S. Hashimoto, Y. Iwamoto, S. Noda, T. Ogawa, H. Iwase, H. Nakashima, T. Fukahori, K. Okumura, T. Kai, S. Chiba, T. Furuta, L. Sihver, J. Nucl. Sci. Technol. 50 (2013) 913.
[19] T. Sato, Y. Iwamoto, S. Hashimoto, T. Ogawa, T. Furuta, S. Abe, T. Kai, P.-E. Tsai, N. Matsuda, H. Iwase, N. Shigyo, L. Sihver, K. Niita, J. Nucl. Sci. Technol. 555 (2018) 684.
[20] P. Kirkegaard, J. V. Olsen, M. M. Eldrup, PALSfit3: A software package for analyzing positron lifetime spectra, Technical University of Denmark, DTU (2017).
[21] J. V. Olsen, P. Kirkegaard, N. J. Pedersen, M. Eldrup, phys. stat. sol. (c) 4 (2007) 4004.
[22] B. Bergersen, M. J. Stott, Solid State Commun. 7 (1969) 1203.
[23] D. C. Connors, R. N. West, Phys. Lett. 30A (1969) 24.
[24] A. Seeger, Appl. Phys. 4 (1974) 183.
[25] X. Gonze, G.-M. Rignanese, M. Verstraete, J.-M. Beuken, Y. Pouillon, R. Caracas, F. Jollet, M. Torrent, G. Zerah, M. Mikami, P. Ghosez, M. Veithen, J.-Y. Raty, V. Olevano, F. Bruneval, L. Reining, R. Godby, G. Onida, D. R. Hamann, D. C. Allan, Z. Kristallogr. 220 (2005) 558.
[26] X. Gonze, B. Amadon, P.-M. Anglade, J.-M. Beuken, F. Bottin, P. Boulanger, F. Bruneval, D. Caliste, R. Caracas, M. Côté, T. Deutsch, L. Genovese, P. Ghosez, M. Giantomassi, S. Goedecker, D. R. Hamann, P. Hermet, F. Jollet, G. Jomard, S. Leroux, M. Mancini, S. Mazevet, M. J. T. Oliveira, G. Onida, Y. Pouillon, T. Rangel, G.-M. Rignanese, D. Sangalli, R. Shaltaf, M. Torrent, M. J. Verstraete, G. Zerah, J. W. Zwanziger, Comput. Phys. Commun. 180 (2009) 2582.
[27] X. Gonze, F. Jollet, F. A. Araujo, D. Adams, B. Amadon, T. Applencourt, C. Audouze, J.-M. Beuken, J. Bieder, A. Bokhanchuk, E. Bousquet, F. Bruneval, D. Caliste, M. Côté, F. Dahm, F. D. Pieve, M. Delaveau, M. D. Gennaro, B. Dorado, C. Espejo, G. Geneste, L. Genovese, A. Gerossier, M. Giantomassi, Y. Gillet, D. R. Hamann, L. He, G. Jomard, J. L. Janssen, S. L. Roux, A. Levitt, A. Lherbier, F. Liu, I. Lukačević, A. Martin, C. Martins, M. J. T. Oliveira, S. Poncé, Y. Pouillon, T. Rangel, G.-M. Rignanese, A. H. Romero, B. Rousseau, O. Rubel, A. A. Shukri, M. Stankovski, M. Torrent, M. J. V. Setten, B. V. Troeye, M. J. Verstraete, D. Waroquiers, J. Wiktor, B. Xu, A. Zhou, J. W. Zwanziger, Comput. Phys. Commun. 205 (2016) 106.
[28] M. Torrent, F. Jollet, F. Bottin, G. Zérah, X. Gonze, Comput. Mater. Sci. 42 (2008) 337.
[29] M. A. L. Marques, M. J. T. Oliveira, T. Burnus, Comput. Phys. Commun. 183 (2012) 2272.
[30] P. E. Blöchl, Phys. Rev. B 50 (1994) 17953.
[31] J. P. Perdew, K. Burke, M. Ernzerhof, Phys. Rev. Lett. 77 (1996) 3865.
[32] J. Wiktor, G. Jomard, M. Torrent, M. Bertolus, Phys. Rev. B 87 (2013) 235207.
[33] J. Wiktor, G. Jomard, M. Torrent, Phys. Rev. B 92 (2015) 125113.
[34] M. J. Puska, A. P. Seitsonen, R. M. Nieminen, Phys. Rev. B 52 (1995) 10947.
[35] K. Momma, F. Izumi, J. Appl. Cryst. 44 (2011) 1272.
[36] H. E. Beske, Microchim. Acta 91 (1987) 309.
[37] X.-S. Kong, Y.-W. You, C. Song, Q. F. Fang, J.-L. Chen, G.-N. Luo, C. S. Liu, J. Nucl. Mater. 430 (2012) 270.
[38] H.-E. Schaefer, Phys. Status Solidi A 102 (1987) 47.
[39] P. M. G. Nambissan, P. Sen, Radiat. Eff. 124 (1992) 215.
[40] T. E. M. Staab, R. Krause-Rehberg, B. Vetter, B. K. G. Lange, P. Klimanek, J. Phys.: Condens. Matter 11 (1999) 1787.
[41] S. Zhu, Y. Xu, Z. Wang, Y. Zheng, D. Zhou, E. Du, D. Yuan, M. Fukuda, M. Mihara, K. Matsuta, T. Minamisono, J. Nucl. Mater. 343 (2005) 330.
[42] A. Seeger, F. Banhart, Phys. Status Solidi A 102 (1987) 171.
[43] K. Heinola, T. Ahlgren, J. Appl. Phys. 107 (2010) 113531.
[44] Y.-L. Liu, H.-B. Zhou, Y. Zhang, G.-H. Lu, G.-N. Luo, Comput. Mater. Sci. 50 (2011) 3213.
[45] Y.-L. Liu, Z.-H. Dai, W.-T. Wang, Comput. Mater. Sci. 83 (2014) 1.
[46] Y.-L. Liu, S. Jin, Y. Zhang, Chin. Phys. B 21 (2012) 016105.
[47] A. Alkhamees, Y.-L. Liu, H.-B. Zhou, S. Jin, Y. Zhang, G.-H. Lu, J. Nucl. Mater. 393 (2009) 508.
[48] S. Fukuzumi, T. Yoshiie, Y. Satoh, Q. Xu, H. Mori, M. Kawai, J. Nucl. Mater. 343 (2005) 308.
[49] K. Ohsawa, J. Goto, M. Yamakami, M. Yamaguchi, M. Yagi, Phys. Rev. B 82 (2010) 184117.
[50] D. F. Johnson, E. A. Carter, J. Mater. Res. 25 (2010) 315.
[51] K. Heinola, T. Ahlgren, K. Nordlund, J. Keinonen, Phys. Rev. B 82 (2010) 094102.